JOURNAL OF GEOPHYSICAL RESEARCH, VOL. 115, B07102, doi:10.1029/2009JB006986, 2010

Thermally stimulated "runaway" downhole flow in a superhydrostatic ocean crustal borehole: Observations, simulations, and inferences regarding crustal permeability

Earl E. Davis,[1] Alison LaBonte,[1,2] Jiangheng He,[1] Keir Becker,[3] and Andrew Fisher[4]

Received 17 September 2009; revised 8 February 2010; accepted 15 March 2010; published 14 July 2010.

[1] An array of boreholes, drilled through a regionally continuous hydrologically confining layer of sediments into extrusive igneous basement rocks of the Juan de Fuca Ridge eastern flank, has been instrumented with CORK hydrologic observatories for long-term monitoring and fluid sampling. Omission of seals between nested casing strings reaching into basement at one site created a low-resistance connection between basement and the overlying water column, and despite the natural superhydrostatic state of basement water at that location, a "runaway" condition of cold seawater downhole flow into the crust was established, which persisted for more than 4 years. The existence of this condition, along with perturbations generated by it and by initial drilling operations observed at a properly sealed hole 2.4 km away, have been used with analytic and finite element model solutions to constrain formation permeability. The minimum threshold permeability allowing stable downhole flow is roughly 4×10^{-13} m^2. A value of permeability similar to this ($3–4 \times 10^{-13}$ m^2) is estimated on the basis of the elapsed time for initial perturbations to propagate between the sites (~2.5 days). The amplitude of the long-term flow perturbation observed at the sealed site (roughly 1.7 kPa) is smaller than that predicted by modeling (5–10 kPa). Models for flow in an anisotropically permeable layer show that this could be the consequence of low vertical permeability (e.g., arising from massive volcanic or sediment interlayering) or high permeability in the direction of the tectonic fabric generated at the ridge axis. Disagreement between the permeabilities estimated here with previous large-scale estimates appropriate for the cross-strike direction (the primary direction between the borehole sites) (10^{-10}–10^{-9} m^2) is difficult to reconcile; it is possible that the holes are poorly connected to zones of high permeability that facilitate the large lateral fluid and heat fluxes previously inferred at this young crustal site.

Citation: Davis, E. E., A. LaBonte, J. He, K. Becker, and A. Fisher (2010), Thermally stimulated "runaway" downhole flow in a superhydrostatic ocean crustal borehole: Observations, simulations, and inferences regarding crustal permeability, *J. Geophys. Res.*, *115*, B07102, doi:10.1029/2009JB006986.

1. Introduction

[2] Boreholes drilled through sediments and into young igneous oceanic crust are commonly observed to create hydrologic short circuits through layers of low-permeability sediment. In many instances, borehole temperature profiles collected shortly after drilling have shown the effects of fluid flow, both uphole and downhole, from or into permeable basement intervals (Deep Sea Drilling Project (DSDP) and Ocean Drilling Program (ODP) holes 395A, 482C, 504B, 857D, 858G, 1024C, 1025C, 1026B, 1027C, 896C), and where boreholes have remained open, flow has been observed to persist for years (holes 395A, 504B) [*Duennebier et al.*, 1983; *Becker et al.*, 1984, 1985; *Gable et al.*, 1989; *Morin et al.*, 1992]. Early recognition of this problem motivated the development of what became known as the "circulation obviation retrofit kit" or CORK, an instrumented seal designed to prohibit borehole flow and allow natural formation pressures and temperatures to be determined after drilling and open-hole perturbations had dissipated [*Davis et al.*, 1992]. A number of installations have been carried out in ridge axis and ridge flank environments, some in holes drilled with observatory installations being a primary objective (holes 857D, 858G, 1024C, 1025C,

[1]Pacific Geoscience Center, Geological Survey of Canada, Sidney, British Columbia, Canada.
[2]Now at Office of Energy Efficiency and Renewable Energy, U.S. Department of Energy, Washington, DC, USA.
[3]Rosenstiel School of Marine and Atmospheric Science, University of Miami, Miami, Florida, USA.
[4]Earth and Planetary Sciences Department, University of California, Santa Cruz, California, USA.

0148-0227/10/2009JB006986

1026B, 1027C) and some in preexisting holes that were known to host long-term flow (holes 395A, 504B, 896A) [*Davis and Becker*, 1994; *Davis et al.*, 1997; *Becker et al.*, 2001, 2004]. From pressure and temperature observations in these CORKed holes, along with knowledge of the local lithologic, thermal, and geochemical structure from seismic, seafloor heat flux and interstitial water composition data, a consistent pattern has emerged in which very small lateral pressure differentials (a few kilopascals or less, relative to the commonly isothermal hydrostats within basement) drive rapid fluid flow in the uppermost crust. Where there is significant basement relief, substantial pressure differentials develop across the blanketing sediment sections [*Davis and Becker*, 1994, 2002, 2004]. Superhydrostatic conditions (relative to the local sediment geotherm) are present at buried basement ridges and other edifices (e.g., sites 858, 896, 1025, 1026), whereas subhydrostatic conditions are present in basement valleys (e.g., sites 395, 504, 1024, 1027). The vertical pressure differentials cause slow seepage through blanketing sediment cover [e.g., *Mottl*, 1989; *Davis et al.*, 1992; *Wheat and Mottl*, 1994] and contribute to the driving forces for upward and downward flow in unsealed holes. In instances where rates of borehole flow were measured or estimated from perturbed temperature profiles and seafloor-to-formation pressure differentials were estimated or measured immediately after holes were sealed, average permeabilities of the basement sections producing or absorbing the flow could be calculated [*Becker et al.*, 1994; *Fisher et al.*, 1997; *Becker and Davis*, 2003].

[3] During Integrated Ocean Drilling Program (IODP) Expedition 301, two new holes, 1301A and 1301B, were drilled into a basement ridge on the young (3.5 Ma) but thickly sedimented eastern flank of the Juan de Fuca Ridge [*Fisher et al.*, 2005] where superhydrostatic pressures had been observed [*Davis and Becker*, 2002]. The new CORK installations were completed with the goals of documenting the hydrogeology parallel to the local crustal structure (to complement what had been learned from holes 1026B and 1027C, drilled across strike from one another and instrumented during ODP Leg 168) and studying the heterogeneity of the crust at levels deeper than had been reached previously. Unfortunately, the new holes were not properly sealed, which resulted in long-term and relatively unimpeded leakage. The ensuing flow was not in the direction expected on the basis of the local superhydrostatic formation state; flow entered the formation through both holes, and this flow persisted for several years. In this paper, we summarize the observations at these CORKed holes and discuss the results of a numerical simulation that shows the conditions under which stable downhole flow into naturally overpressured basement can occur. The primary parameters controlling the history of flow (beyond the magnitude of local natural overpressure) are the depth into basement penetrated by the borehole and basement permeability. The work is complementary to an analysis by *Fisher et al.* [2008] based on a portion of the same data set.

2. Hydrologic Setting and the "Rough Basement" Borehole Observatory Array

[4] Four CORKed boreholes have been established in a detailed hydrologic study of sediment-buried basement on the eastern flank of the Juan de Fuca Ridge, two in 1996 during ODP Leg 168 (holes 1026B and 1027C) and two in 2004 during IODP Expedition 301 (holes 1301A and 1301B) [*Davis et al.*, 1997; *Fisher et al.*, 2005]. The igneous crust in this area is rugged but thickly and extensively sedimented, with the exception of three small seamounts (Mama, Papa, and Baby Bare) that rise above the local turbidite surface (Figure 1). A detailed description of these boreholes can be found in the work of *Fisher et al.* [2008]. In brief, the hole array (Figures 1 and 2) comprises as follows: (1) Hole 1026B, drilled through 247 m of low-permeability sediments and 48 m of extrusive igneous rocks along a sediment-buried basement ridge (Figure 1b). Uppermost basement water at this site is positively pressurized relative to the local geothermal hydrostat by roughly 18 kPa [*Davis and Becker*, 2002]. (2) Hole 1027C, drilled 2.2 km to the east in a neighboring buried basement valley (Figure 1b) through 614 m of sediment and a deep intercalated igneous sill and 18 m into extrusive igneous crust. Uppermost basement fluid pressure at this site is 26 kPa below the locally defined geothermal hydrostat but virtually identical to that at hole 1026B when compared using the isothermal fluid density basement pathway that connects the two holes [*Davis and Becker*, 2002]. (3) Hole 1301A, drilled roughly 1 km SSW of hole 1026B (along strike of the buried ridge) through 262 m of sediment and 105 m into the uppermost igneous crust. (4) Hole 1301B, drilled 50 m north of 1301A through 265 m of sediment and 318 m of extrusive basalts. On the basis of knowledge of the hydrologic regime and constraints from previous observations at hole 1026B, the uppermost crust at holes 1301A and 1301B is expected to be overpressured relative to the local geotherm hydrostat by roughly 16 kPa. These holes penetrate considerably deeper than the depth reached by hole 1026B, however, and may access contrasting hydrologic regimes.

[5] At holes 1026B, 1027C, and 1301A, pressures are measured in single basement intervals between the base of casing and the bottom of the holes (Figure 2). In addition, a monitoring interval was established within the cased section of hole 1301A (between the seafloor CORK casing seal and a packer set near the bottom of the 10 3/4″ casing) to evaluate the quality of the packer seal. At hole 1301B, three basement intervals were established with two packers set in basement.

[6] Unfortunately, not all of these holes have been completely sealed. Hole 1026B leaked from the time monitoring began in 1996, with discharge of warm water occurring until the hole was refurbished with a new CORK during Expedition 301. A better seal was achieved with the 2004 installation, although temperature variations and accumulations of bacterial growth at the wellhead and recent downhole thermal data show a slow leak to be present, probably at the seal between the CORK structure and the 10 3/4″ casing. At holes 1301A and 1301B, the situation is far worse. A design error precluded the deployment of a critical seal between a nested pair of borehole casings (16″ and 10 3/4″ OD) that extend in each of the holes from the seafloor into upper basement (see Figure 2), and this resulted in major leaks. As a result, a long-term perturbation experiment was unknowingly initiated, with leakage into the formation at holes 1301A and 1301B creating a long-lived perturbation (see section 3). An attempt to seal

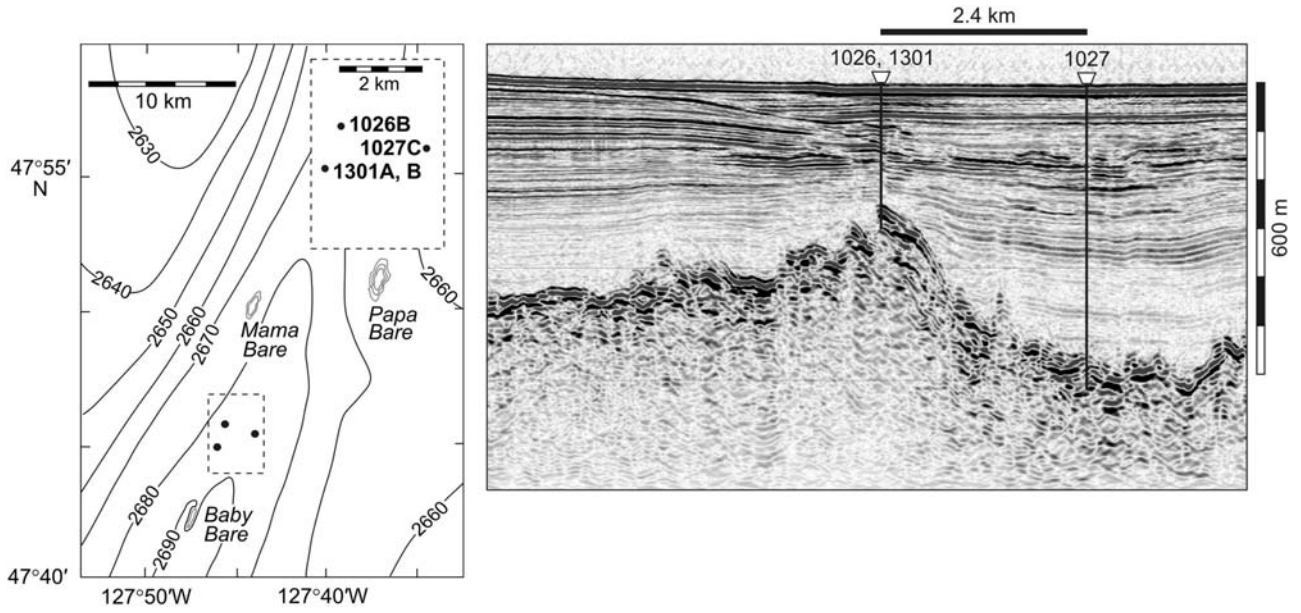

Figure 1. (a) Map of the vicinity of instrumented boreholes on the eastern Juan de Fuca Ridge flank that are the focus of this study, with water depths in meters. The oceanic crust is sealed by a thick blanket of low-permeability sediments except at the three named small isolated basement outcrops. Extensive basement outcrops occur only near the axis of the Juan de Fuca Ridge axis roughly 80 km to the west. (b) Seismic section crossing the strike of the buried crustal structure, directly over holes 1026A and 1027B. Seafloor water depths and location of holes are given on map in Figure 1a.

hole 1301B with a small amount of cement pumped into the reentry cone was made during the drilling expedition, but this was unsuccessful. A later attempt to plug the leak was made at hole 1301B in 2007 using the submersible Alvin, this time with cement containing a filler; flow was reduced but not stopped. In 2009, quantities of cement sufficient to fill the reentry cones 3 times over were delivered to both holes by the drilling vessel Resolution. Hole 1301B appears to have been at least partly sealed by this operation, whereas hole 1301A continues to vent warm formation fluid.

[7] Hole 1027C remained well sealed from the time of its installation in 1996 until late 2007 (when a leak developed through an incompletely mated hydraulic connector). Pressure recorded in this hole during and following the drilling activities of Expedition 301 provided the basis for an unplanned cross-hole permeability test that used an estimate of the perturbation at hole 1301B as a source [*Fisher et al.*, 2008]. The hole 1027C record also provides constraints for the expanded modeling effort described below.

3. Observations and First-Order Inferences

3.1. Long-Term Histories

[8] Long-term pressure records (with diurnal and semidiurnal tidal signals removed) from each of the holes are shown in Figure 3. Seafloor and formation pressures were monitored at hole 1027C continuously before, during, and after IODP Expedition 301 drilling and CORKing activities. Sensors were installed at holes 1026B, 1301A, and 1301B a few weeks after Expedition 301 drilling and CORK installations were completed. There was a hiatus in the records from holes 1026B, 1301A, and 1301B between the beginning of 2006, when a software problem caused the instruments to stop logging, and September 2007 when the problem was rectified. From late 2007 to mid-2008, formation pressure was not recorded at hole 1027C when the hydraulic coupler of a piggyback sensor/logger package failed to mate properly. This problem was rectified at the time of a site visit in August 2008.

[9] The records show contrasting histories, and all bear witness to various forms of leakage. Pressure in hole 1026B (Figure 3a) was roughly +41 kPa (superhydrostatic) after instrument installation, then decayed ultimately toward the level estimated from post-Leg 168 monitoring of roughly +18 kPa. A secondary transient followed a site visit in 2005, when a large-diameter microbiological fluid sampling valve was opened. Pressure in hole 1027C (Figure 3b) was stable at a level of roughly −26 kPa (subhydrostatic) before Expedition 301 operations, then increased thereafter, climbing by about 1.7 kPa by mid-2007. Pressures in the two intervals in hole 1301A (Figure 3c) track one another closely through the end of the initial recording period. They are initially slightly subhydrostatic (by less than 1 kPa) and climb to slightly superhydrostatic (also by less than 1 kPa). After loggers were restarted in 2007, pressure recorded at the lower screen had climbed to roughly +10 kPa while the upper interval remained close to hydrostatic, and pressures at both levels displayed large short-term variations. Pressures at each of the three intervals in hole 1301B (Figure 3d) were substantially below hydrostatic throughout the recording history. A significant change occurred when the attempt was made to seal the leaking casing hanger with cement in 2007; pressures became even more strongly subhydrostatic

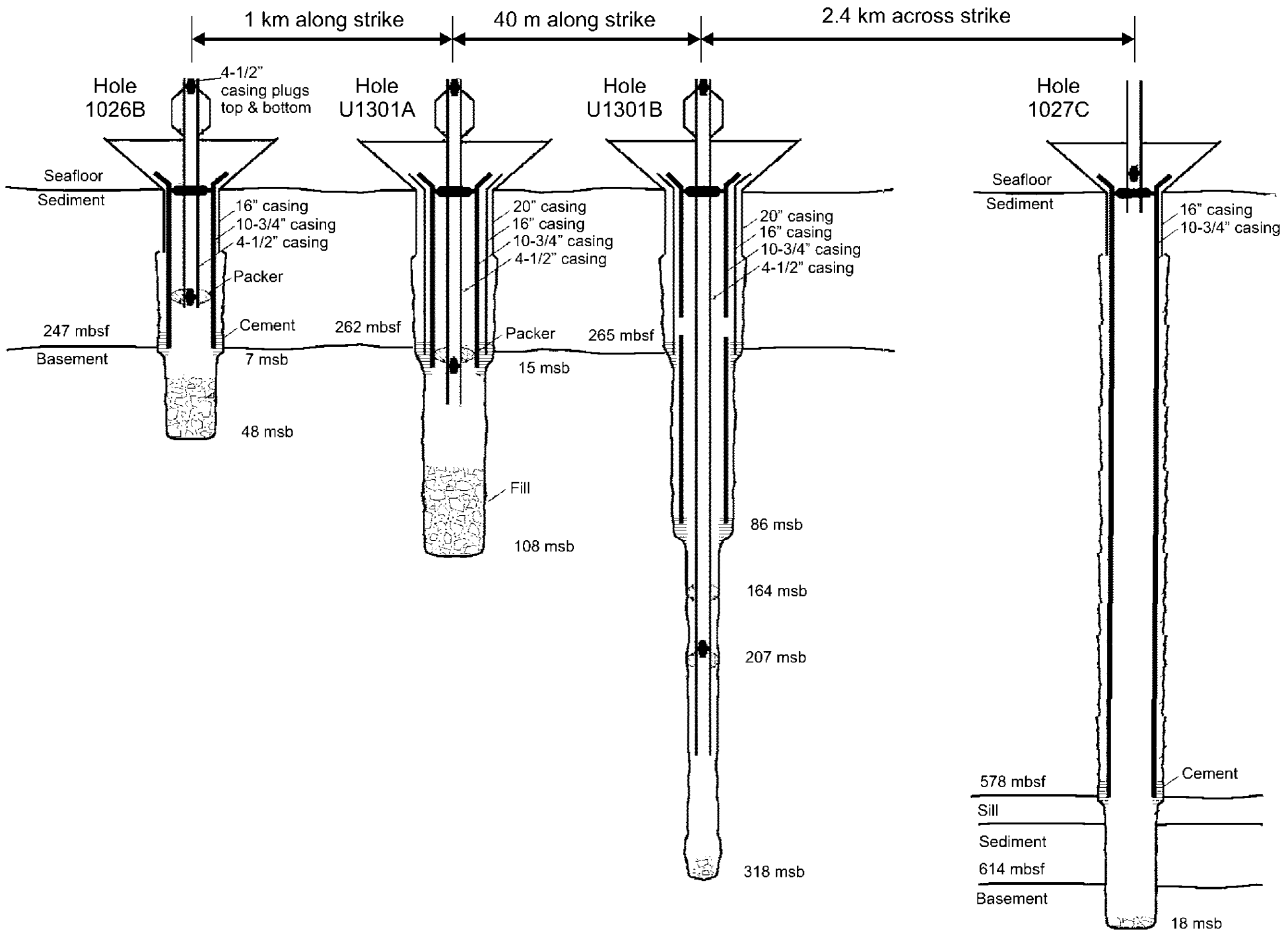

Figure 2. Borehole and CORK schematics for holes 1026B, 1027C, 1301A, and 1301B. Lack of seals between the 10 3/4″ and 16″ casing hangers at holes 1301A and 1301B allowed leakage between the seafloor and basement via the annular gap between the two casing strings. Collapse of sediment around the 10 3/4″ casings and limited penetration into basement prior to cementing operations appear to have produced tight hydrologic barriers between basement and the seafloor at holes 1026B and 1027C. This was probably not the case in holes 1301A and 1301B, where cement was probably lost to the formation, and sediment collapse against the 10 3/4″ casing was prevented by the 16″ casing. Depths are given in meters below seafloor (mbsf) and meters sub-basement (msb).

until the data download in 2008. Pressures at the lower and middle screens were virtually identical to one another throughout the recording periods.

3.2. Effects of Anomalous Buoyancy

[10] To understand these records, it is necessary to consider the consequences of leakage in the context of the hydraulic plumbing of the installations. Under ideal conditions (i.e., full thermal equilibrium with the natural formation state), pressures recorded by sensors at the seafloor via solid casing or hydraulic tubing reflect formation conditions accurately. When open holes or screens penetrate low-permeability material, small leaks can cause major shifts in borehole pressure toward hydrostatic conditions. In high-permeability formations, the direct effects of leakage are smaller, but flow-induced thermal perturbations relative to the natural formation state cause offsets due to anomalous buoyancy of the water in the casing or the umbilical tubing that links seafloor sensors to the formation below. With the sensors being at the top of the hole, cooling caused by downward flow produces negative pressure offsets (the same as putting a thumb on a soda straw), and warming caused by upward flow has the opposite effect. This is true whether flow occurs within one of the casing strings (as is the case in holes 1301A and 1301B and in hole 1026B prior to and to a lesser extent after installation of the new CORK during Expedition 301) or only within the umbilical, where fluid sampling and pressure monitoring lines are in close proximity to one another and are well insulated from the borehole and formation (as is the case in hole 1026B, when the large-diameter fluid sampling line was opened in 2005, causing the pressure monitoring line to be warmed and the measured pressure to increase; Figure 3a). Upper limits for thermally induced pressure perturbations are shown for the case of holes 1301A and 1301B in Figure 4. These are calculated as the contrast between isothermally warm or cold columns relative to the estimated geotherm at site 1301, conductive through the sediment section and isothermal at

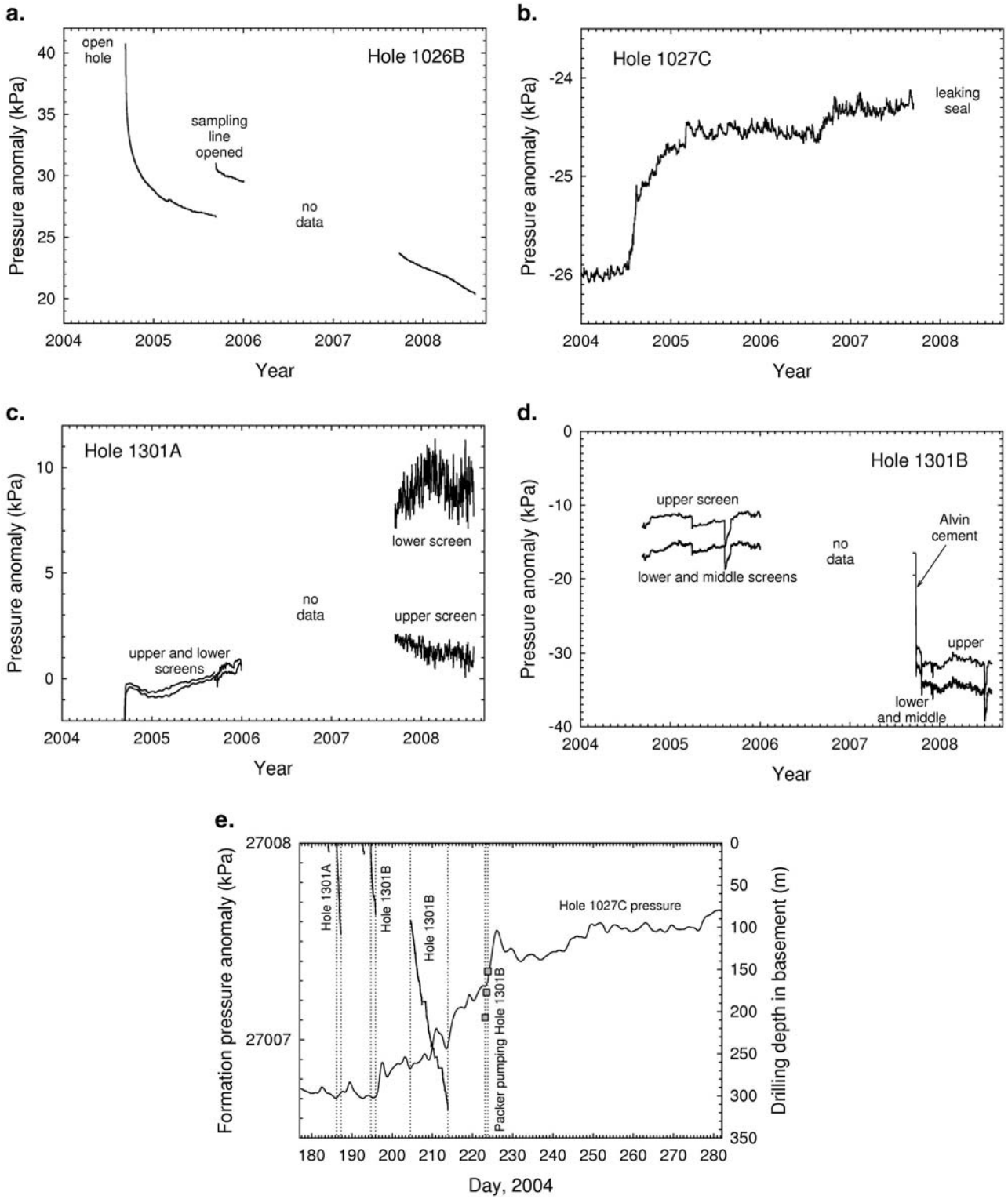

Figure 3. (a) Formation pressure history in hole 1026B, referenced to local seafloor hydrostatic pressure and with effects of tidal loading removed. (b) Pressure history, hole 1027C. (c) Pressure history, hole 1301A. (d) Pressure history, hole 1301B. (e) Early formation pressure history at hole 1027C compared to histories of basement drilling and permeability pumping tests at holes 1301A and 1301B.

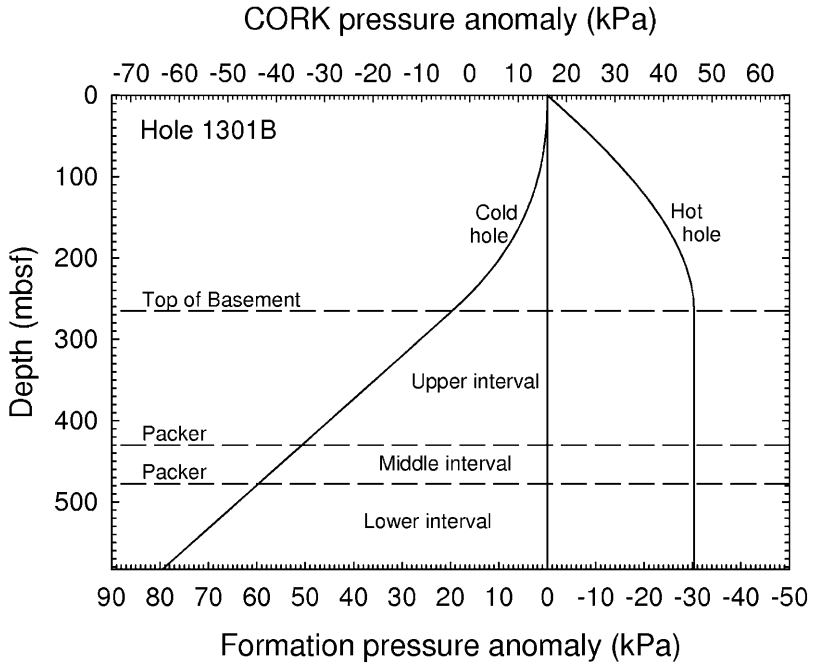

Figure 4. Limiting pressure "profiles" for hole 1301B, plotted relative to the local geothermal hydrostat for the extreme cases of isothermally hot (64°C) and cold (2°C) water discharging from or recharging into isothermally hot igneous basement. The upper axis shows the anomalous pressure across the CORK seafloor seal as a function of the depth of the thermal perturbation and includes the ~16 kPa natural state of the formation. The lower axis is the pressure anomaly "looking up" as seen by the formation. Smaller anomalies would be present if recharge or discharge rates were not sufficient to maintain isothermal conditions, and greater anomalies could be produced if there were a significant thermal gradient in basement.

64°C in basement. Uphole flow is seen to have the potential for augmenting the natural positive differential pressure between the formation and the seafloor by as much as 30 kPa (thus explaining the peak pressure seen in Figure 3a at the time of the beginning of recording at hole 1026B [see also *Davis and Becker*, 2000]). The anomalous buoyancy associated with cooling by rapid drilling circulation or buoyancy-driven downhole flow is of the opposite sign and, at holes 1301A and 1301B, is seen to be large enough to overcome the natural superhydrostatic state by creating a net negative differential between the formation and seafloor, even with minimal penetration into basement. With deeper penetration, the potential to stimulate downhole flow grows, along with the strength of the feedback between flow and its driving force. Viewed from the perspective of the formation, downward flow to the full depth of the hole is seen to be capable of producing a perturbation of over +80 kPa (Figure 4, lower axis). This is believed to be the cause of the post-Expedition 301 transient seen at hole 1027C (Figure 3b).

[11] While the negative signs of the observed pressure anomalies observed by the CORKs in hole 1301B and initially in hole 1301A are useful by way of being clearly diagnostic of downhole flow, it is difficult to draw quantitative conclusions about driving forces for flow from the magnitudes of the negative pressures observed without knowledge of the perturbed thermal structure. The differential pressures observed across the leaky seals reflect an unknown fraction of the thermal buoyancy forces and thus provide only a lower limit of the total thermally derived anomalous pressure driving flow into the basement section. Were the casing hanger restriction great, the observed anomalies would reflect the full magnitude of the buoyancy-derived perturbation, but this degree of restriction would soon put an end to the source of the perturbation (downhole cold water flow) and pressure would recover to the natural superhydrostatic state. If the resistance to flow were insignificant, pressures measured in the boreholes would be hydrostatic (as defined by the thermal structure of the holes themselves), and very little of the chilled hole pressure seen by the formation would be observed by the sensors. The actual situation must lie somewhere in between.

[12] For the initial condition in the analysis in section 3.3, which considers the effects of flow in hole 1301B (hole 1301A is not considered for reasons given later), we assume a situation close to the latter end-member, i.e., that little restriction was created by the installation of the CORK and that initial flow occurred at a sufficiently great rate to cause the hole to be cooled to the temperature of ocean bottom water. This assumption is justified by downhole observations of temperature at the time of packer testing [*Fisher et al.*, 2005; *Becker and Fisher*, 2008]. The pressure seen by basement at the level of the bottom of the hole would have been equal to the full potential created by a cold hole (80 kPa) prior to CORK installation (Figure 4) and this value less the pressure losses across the casing hangers at the seafloor (~7 kPa) and across or around the packers separating the formation monitoring intervals (an additional

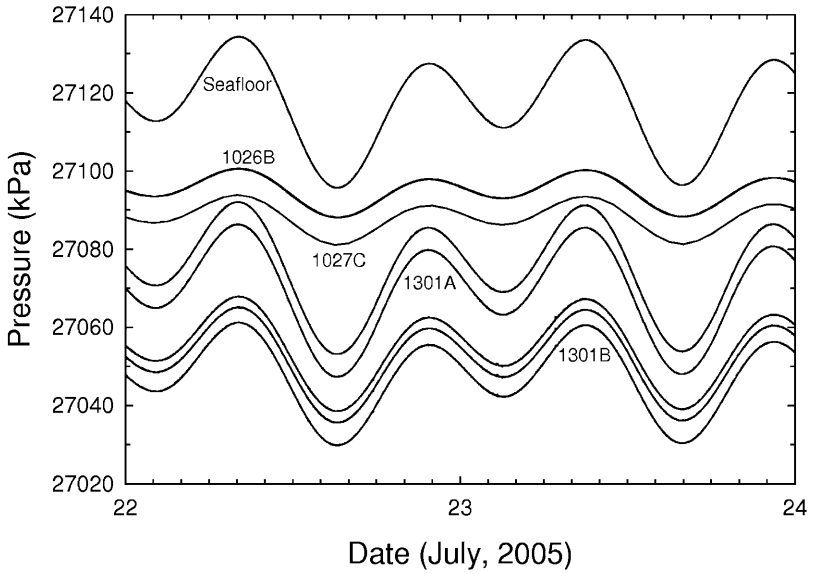

Figure 5. Unfiltered pressures near the end of the recording period at holes 1026B, 1027C, 1301A, and 1301B. Absolute pressure levels have been shifted for plotting convenience.

10 kPa across the upper packer; virtually nothing across the lower) immediately after CORK installation (Figure 3d). Cement emplaced by Alvin in 2007 increased the restriction to flow, but flow was still not restricted sufficiently to allow significant thermal recovery. Pressure became more negative, suggesting that downhole flow continued to maintain an anomalous density column despite the greater loss of pressure through the constriction created by the cement. In the future, temperature data from the CORK sensor/sampler cables will provide valuable constraints on anomalous buoyancy and the rate of flow, but for now, estimation of the actual pressure perturbations produced by the negative thermal buoyancy associated with the downhole flow remains uncertain. If flow were less rapid, the negative thermal buoyancy and associated pressure perturbation would be less; if the natural state is warmer than assumed (i.e., if there is a significant thermal gradient within basement), then the pressure perturbation could be greater. The reversal to uphole flow in hole 1301A that occurred in the third year of monitoring (seen in temperature data to have occurred not long before the 2007 Alvin site visit) is assumed not to have affected the state and flow in hole 1301B; pressures observed in hole 1301B after the 1301A reversal but before Alvin cementing were close to the level seen at the end of the first monitoring period (Figure 3d).

3.3. Perturbation Observed at Hole 1027C

[13] In contrast to the problematic holes 1026B, 1301A, and 1301B, hole 1027C was sealed nearly continuously from the time it was installed in 1996 until 2007. After recovery from the initial transient associated with drilling and open-hole conditions during ODP Leg 168, pressure remained at a nearly constant level (−26 kPa [*Davis and Becker*, 2002]) until Expedition 301 operations (i.e., the level seen in early 2004; Figure 3b). The long-term rise in pressure beginning in 2004 at the time of basement drilling activities at holes 1301A and 1301B is unquestionably anomalous, and the timing indicates a causal link. A closer inspection (Figure 3e; see also discussion in the work of *Fisher et al.* [2008]) reveals important details about this link, namely that drilling to a depth of 108 m sub-basement in hole 1301A had no resolvable effect on pressure at hole 1027C, whereas anomalous increases are seen 2–3 days after drilling both the shallow (to 85 m sub-basement) and deep (to 318 m) basement intervals of hole 1301B, as well as after pumping tests in the deeper part of this hole (below 150–200 m sub-basement).

3.4. Tidal Signals: Constraints on Compressibility and Indications of Leakage

[14] Unfiltered records from each of the holes are seen to be dominated by tidal signals (Figure 5). The degree to which seafloor loads are imposed on pore water in the formation depends on the elastic parameters of the rock constituents, the rock matrix, and the interstitial water. In the absence of diffusion, the loading response defines the one-dimensional loading efficiency [*Wang and Davis*, 1996], a parameter that can be used to estimate the hydrologic storage compressibility of the formation [e.g., *Wang*, 2004], which is needed in the modeling described below. Seafloor loading signals in holes 1026B and 1027C display little indication of diffusion by way of phase shifts, and thus, the ratios between the seafloor loading and formation signals (nearly identical at 0.32 and 0.33 in the two holes, respectively) probably reflect the elastic loading efficiency of the formation accurately. With well-constrained compressibilities of the pore water and solid rock constituents (0.41×10^{-9} Pa^{-1} at 64°C and 0.02×10^{-9} Pa^{-1}, respectively), an assumed porosity of 0.1, and an assumed framework Poisson's ratio of 0.1, the loading efficiency values suggest a framework compressibility of 0.07×10^{-9} Pa^{-1} and a hydraulic storage compressibility of 0.10×10^{-9} Pa^{-1}.

[15] In contrast, the borehole tidal signals in hole 1301A are virtually identical to that at the seafloor, and the signals in 1301B are only slightly attenuated relative to the seafloor

(formation/seafloor amplitude ratios = 0.76, 0.77, 0.81 at the deep, middle, and upper levels, respectively, prior to Alvin cementing (Figure 5) and 0.51, 0.52, and 0.53 after). This suggests that, in the absence of the casing seals, the hydraulic restriction of the CORK casing hangers is insufficient to allow formation signals to be observed (particularly at hole 1301A where remedial cementing was not attempted at the time of drilling) and, furthermore, that the packers isolating the intracrustal zones did not seat properly. It is possible that the crust is so permeable that local contrasts in tidal pressure cannot develop, but the lack of contrast in hole 1301A, where the upper interval lies fully within the 10 3/4″ casing and thus where a very low loading efficiency should be observed, indicates that its packer did not fully inflate and seal. The same is probably true for the others.

4. Modeled Flow and Pressure Perturbations

[16] In this section, we describe the results of finite element and analytic models, the former to (1) examine the conditions under which long-lived downhole flow into the locally superhydrostatic formation through hole 1301B can take place and (2) estimate the hydrologic parameters (namely permeability and the thickness of the transmissive layer involved) that can be constrained by the mere existence of sustained flow and by the long-term transient pressure anomaly observed in hole 1027C, and the latter to (3) estimate the permeability as constrained by the time for transmission of signals from holes 1301B to 1027C indicated in Figure 3e. These approaches differ from that used by *Fisher et al.* [2008], but the results and inferences are complementary.

4.1. Finite Element Model Description and Assumptions

[17] The finite element model for downhole flow and basement recharge assumes axisymmetric flow into a basement aquifer confined above and below by zero permeability material (sediment and impermeable igneous rocks, respectively). Storage compressibility of the aquifer is constrained by the tidal loading efficiency observed at holes 1026B and 1027C as described above; other parameters assumed or constrained by independent observations comprise: fluid compressibility (temperature dependent) = 0.47×10^{-9} Pa^{-1} at 2°C, 0.41×10^{-9} Pa^{-1} at 60°C; sediment thermal conductivity = 1 W m^{-1} K^{-1}; basement thermal conductivity = 300 W m^{-1} K^{-1} (a high value assigned as a proxy for high Nusselt number convective heat transfer); hole diameter = 0.3 m (equivalent to the cross section of the annulus between the nested casing strings where leakage takes place); sediment thickness = 250 m. A range of layer thicknesses was considered to examine the dependence of the basic behavior of flow on hole depth or the depth extent of permeability. In-flowing water is absorbed via the storage compressibility of the basement aquifer, although in some cases, drainage through a distant, locally hydrostatic free-flow boundary was included. Calculations were done using both fully isotropic and transversely isotropic basement permeability, the latter with zero vertical permeability to simulate strongly layered crustal structure. Complications caused by local convective instabilities were prevented by assigning zero thermal expansivity within the basement layer, but vigorous convective heat transfer was simulated via the high thermal conductivity/high Nusselt number proxy. Heat is exchanged conductively between the formation matrix and the water flowing down the hole and into the basement layer. In all cases, the formation away from the boreholes was assigned an isothermally warm (65°C) initial thermal state consistent with drilling observations [*Davis et al.*, 1997; *Davis and Becker*, 2002; *Fisher et al.*, 2005]. The initial pressure state of the basement aquifer was set at +16 kPa (estimated from the +18 kPa pressure at hole 1026B, with the differences in depth to basement and sediment section thermal structure between sites 1026 and 1301 accounted for). This state is felt to be well constrained, so the response over a range of formation pressure values was not explored. The initial thermal state of the borehole was defined to be isothermal at the temperature of bottom water (2°C). The pressure anomaly driving flow at any given time was determined by the buoyancy of the anomalously cool (in the case of downflow) or warm (upflow) borehole relative to the surrounding formation. The initial pressure anomaly would be less than that assumed if the initial drilling circulation or flow were too slow to keep the full extent of the hole cold or greater if flow were to penetrate vertically below the total depth of the hole or to occur in the presence of a significant thermal gradient in the basement layer. A range of model domain radial dimensions was used in initial tests. Results presented here include only those for a domain sufficiently large to cause the boundary effects not to be felt and for a domain with a free-flow boundary at 150 km to simulate in a very approximate way ventilation through unsedimented crust near the ridge axis. A more realistic geometry with a linear near-ridge free-flow boundary or one that included the potentially significant effects of the isolated basement outcrops at Baby Bare and Mama Bare seamounts roughly 5 km to the south and 10 km to the north of site 1301, respectively (Figure 1), was beyond the capability of the axisymmetric model.

4.2. Model Results for the Leaking Holes and Inferences From Observations

[18] The history and consequences of flow into the crust predicted by the finite element model are shown for a range of permeabilities and layer thicknesses in Figures 6–10. In all cases, the rate of downhole flow declines from an initial maximum value as the growing integrated hydraulic resistance of the formation to flow is felt, and as the descending water is heated by conduction from the formation, becomes less dense, and looses its negative buoyancy. This history is typified by the case shown in Figure 6 for a 330 m thick layer. The rate of initial flow is permeability dependent (Figure 7a) and subsequently declines (Figure 6). At low permeabilities, the waning negative buoyancy generated by the waning downhole flow soon becomes less than required to overcome the natural overpressure of the formation, causing flow to reverse. The rate of flow at which this occurs depends weakly on the layer thickness (a factor controlling the buoyancy force), and is roughly constant over the range of permeability where reversal occurs (~0.005 m s^{-1} = 0.4 L s^{-1}; dashed line in Figure 7b). After

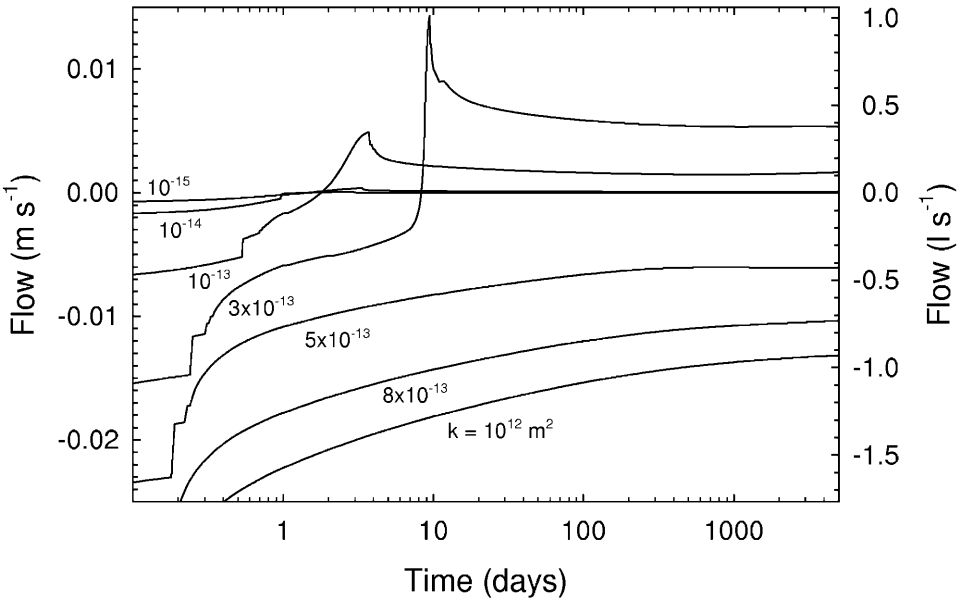

Figure 6. Computed borehole flow history for a 330 m thick basement layer for a range of permeability. Results for fully and transversely isotropic permeability are identical in this plot and in Figures 7–9. Negative values indicate downward flow.

reversal, uphole flow is driven by a combination of the natural formation overpressure and the positive buoyancy of the warm ascending water, plus at early postreversal times by elastic rebound of the aquifer that is charged by prereversal inflow (seen in Figure 6 as a short-lived postreversal peak in flow). At low permeabilities, the time taken for flow to reverse is weakly dependent on layer thickness and permeability (Figure 8). The reversal time increases rapidly as permeability approaches a threshold, however. Above this threshold, downhole flow driven by the negative buoyancy of the cool water in the hole persists at a rate that advectively overpowers conductive heat flow into the hole and flow never reverses (calculations were performed to times of 10,000 days, and only in small domains with a no-flow peripheral boundary condition did flow eventually reverse). The threshold permeability for runaway flow (points falling on dashed line in Figure 7b) is seen to vary inversely with the square of layer thickness (Figure 9). At long times, uphole or downhole flow approaches a rate that is roughly proportional to permeability (Figure 7b) and to the square of layer thickness (Figure 10). The effects of the distant boundary condition are also important at long times (e.g., dashed lines in Figure 11), but this was not explored in a systematic way.

[19] The fact that downhole flow in hole 1301B persisted for more than 4 years sets a lower limit on basement permeability at roughly 4×10^{-13} m^2 for the upper 330 m of the igneous section at that location or higher if permeability is restricted to levels above the bottom of the hole (Figures 8 and 9). That flow reversed in hole 1301A suggests that the permeability of the 108 m basement section penetrated there is less than 3×10^{-12} m^2. In the strict context of the summary of model results shown in Figure 8, the time that transpired before reversal (3 years) is very long. It is possible that the permeability at this hole is simply very close to the threshold for reversal, but it is more likely that the strong downflow in the nearby hole 1301B influenced the thermal and pressure state at hole 1301A; without this influence, hole 1301A may have reversed sooner.

4.3. Model Results for the Far-Field Perturbation and Inferences From Observations

[20] An independent constraint on basement permeability is available from the pressure anomaly generated at site 1301 and observed at hole 1027C situated 2.4 km away (Figure 3b). *Fisher et al.* [2008] employed this constraint by matching the hole 1027C record with the results of an analytical method for computing the radially dependent effects of injection in a test well [*Theis*, 1935]. That domain geometry is similar to the one employed in this paper, but there are important differences in the simulations. For example, the flow in the Theis analysis is fixed (as required by for the analytic solution and assigned by *Fisher et al.* [2008] to fall between 2 and 5 L s^{-1} on the basis of thermal and physical considerations), constant with time, and uniform with depth, whereas in the finite element model used here, flow is computed, varies with time as a consequence of the increasing compression of the aquifer and evolving thermal buoyancy of the water in the borehole, and varies with depth. Only radial diffusion is considered in the Theis formulation, whereas fluid and related pressure signals can diffuse vertically as well as radially in the model used here.

[21] The history of pressure predicted at a given distance from the borehole (Figure 11) follows a sequence consistent with that predicted by the Theis formulation, with pressure beginning to rise after a period of time that depends on permeability and by an amount that also depends on permeability. In cases where a free-flow boundary condition

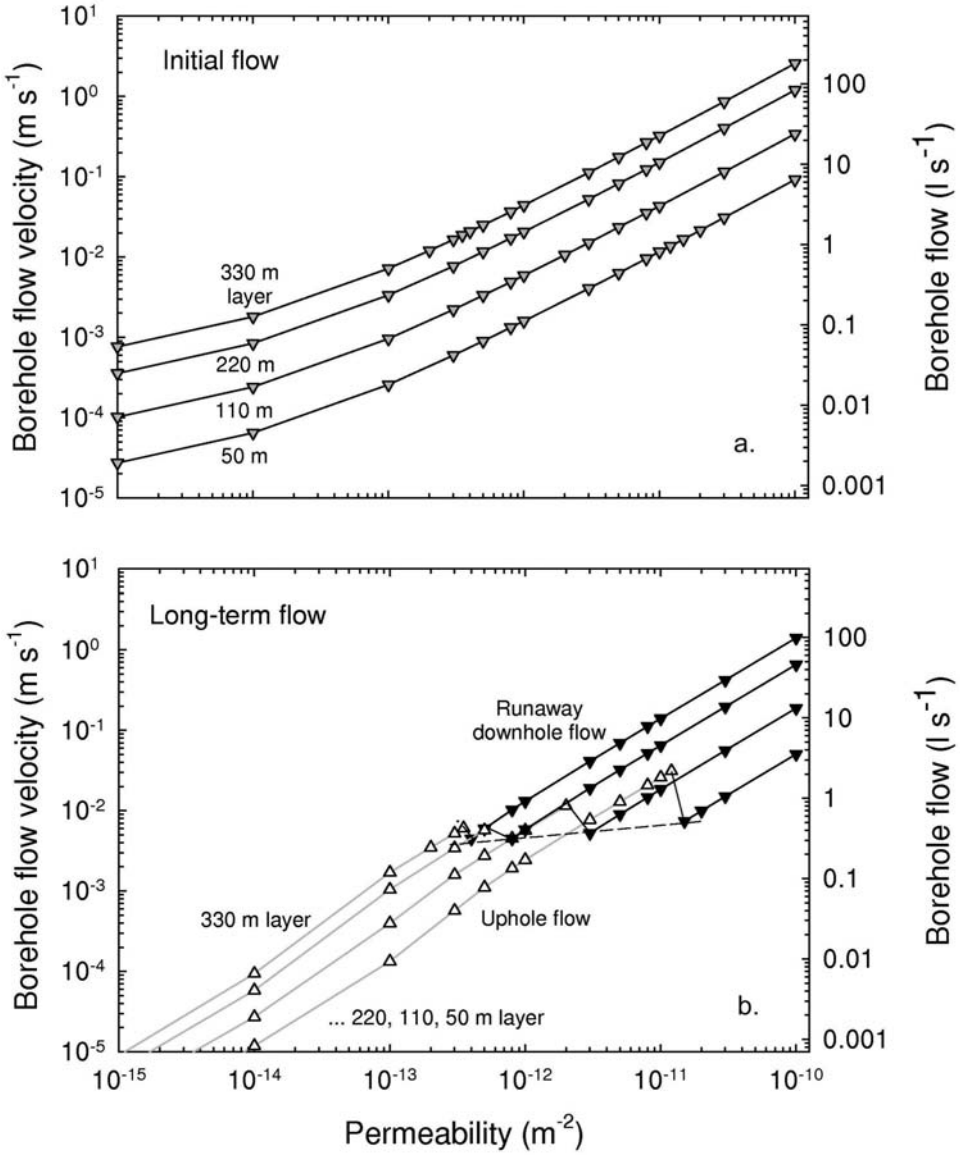

Figure 7. Absolute rate of (a) initial and (b) long-time (steady state) borehole flow as a function of permeability and layer thickness. All initial values are downward; long-time flow is either upward or downward, depending on permeability (upward- and downward-pointing triangles, respectively).

was employed, the effect of ventilation is felt at long times and pressure stabilizes (dashed lines in Figure 11). The level of stability depends on the thickness of the permeable layer and distance to the free-flow boundary, and the time at which the influence begins to be seen depends on the distance to the free boundary and permeability. At permeabilities below the threshold for runaway flow, the pressure perturbation at the monitoring location changes sign after the direction of flow in the leaking hole reverses.

[22] Ideally, comparisons of the observed and modeled pressure histories for each of these phases would provide a suite of constraints on permeability, although complications stand in the way of a robust quantitative interpretation of the record at early and late times. At late times, the effects of ventilation through the extensive igneous outcrops near the ridge axis and through the small but closer "Bares" seamounts will unquestionably have an effect on the way recharge at 1301 affects formation pressure in the vicinity. Complications affect the early-time perturbation history as well. For example, comparison of the onset and initial rise of the perturbation at hole 1027C with the drilling history at site 1301 shows the total drilling history to be protracted (~1 month) relative to the transmission time predicted for typical crustal permeabilities (days down to a fraction of a day; Figure 11), and this precludes use of this model that assumes a simple sudden onset of cooling-induced downhole flow. Furthermore, calculating the rate of flow at early times based on thermal buoyancy alone is only partially correct, given that the circulation rate used during drilling (~50 L s^{-1}) was much greater than the initial buoyancy-driven flow calculated by the model (except at high basement permeabilities; see Figure 7a). The majority of drilling

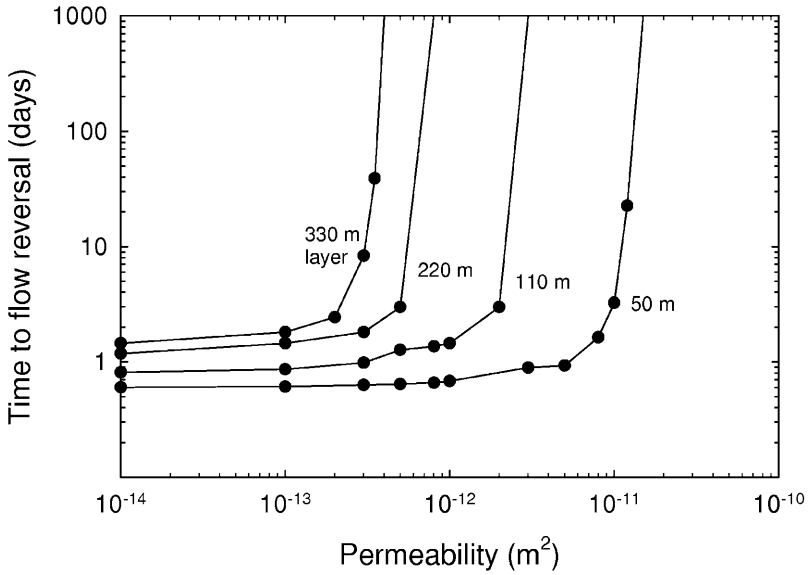

Figure 8. Time taken for modeled borehole flow to reverse as a function of permeability and layer thickness.

circulation may have discharged at the seafloor, but resistance to flow in the annulus between the exterior of the drill pipe and the formation, along with the work exerted to lift drilling debris, probably caused significant pressure to be applied to the formation. Pumps driving drilling circulation operated at ~9 MPa, and although some fraction of this pressure would have been lost to the resistance of flow through the drill bit, there was potential for a much greater forcing than the maximum of 80 kPa that could be generated by thermal buoyancy (Figure 4). Good use can be made of the transit times for the discrete signals generated during hole 1301B drilling operations, however. This is done by use of an analytic solution as described in section 4.4.

[23] Once sufficient time has transpired, the complications at early time should become unimportant, so at intermediate times (>1 month) a comparison of the finite element model results and the observations is warranted and interesting. On the basis of the results for layers with isotropic permeability, it would appear that no reasonable match can be made to the observed perturbation history at hole 1027C.

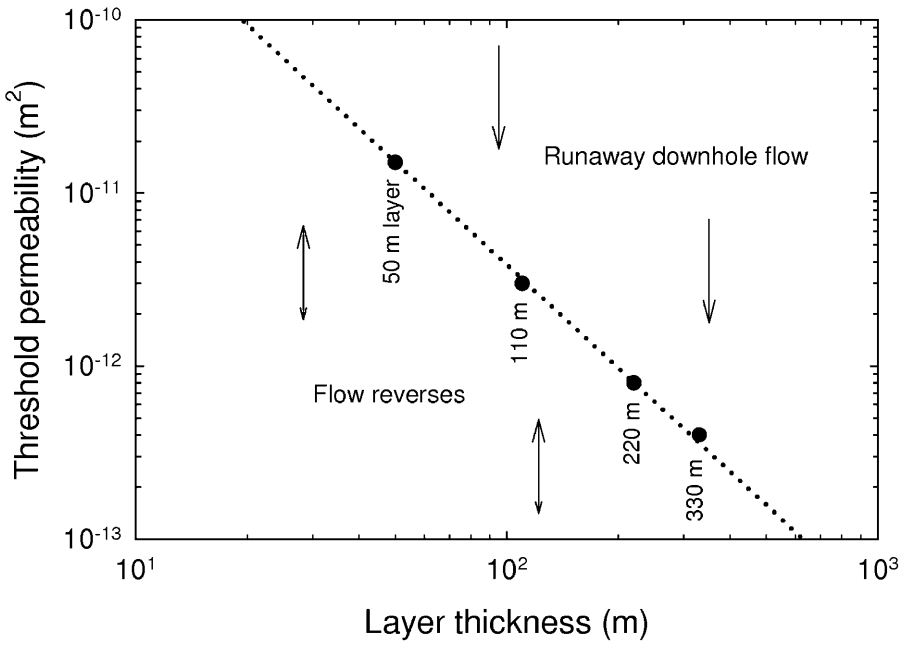

Figure 9. Threshold permeability for "runaway" downhole flow as a function of layer thickness as estimated from the finite element model described in the text.

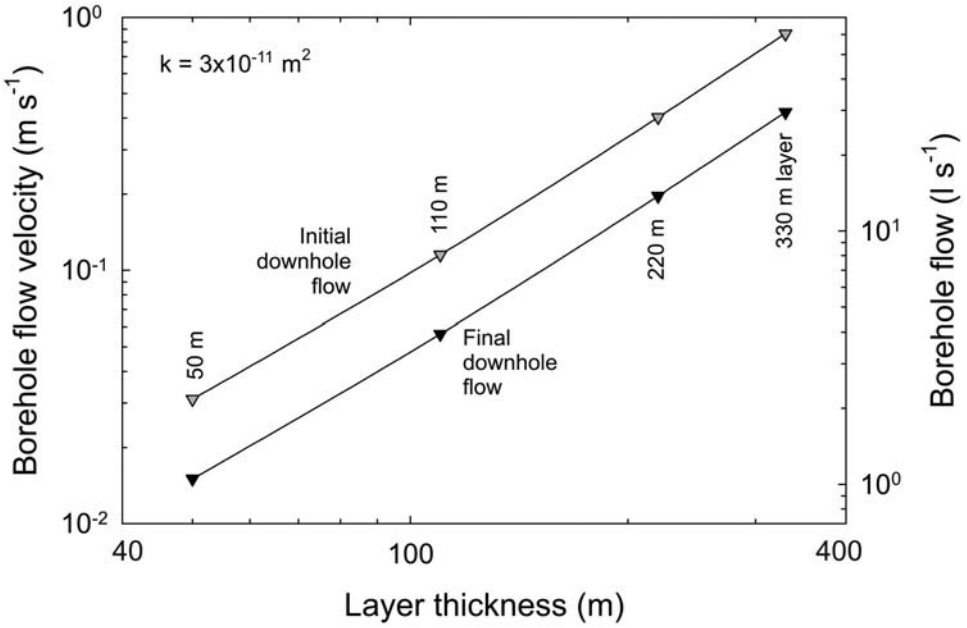

Figure 10. Model-estimated initial and long-time borehole flow rate as a function of layer thickness for a permeability of 3×10^{-11} m^2 (above the runaway flow threshold for all layer thicknesses).

At permeabilities great enough to permit sustained downhole flow, the perturbations predicted are much too large (cf., Figures 11 and 3b). Smaller amplitude anomalies are predicted when flow is confined to shallower layers, but the conditions for sustained flow are met only with very high permeability, which yield anomaly onsets that are much earlier than observed.

4.4. Effects of Permeability Anisotropy

[24] This contradiction would be resolved if the permeability were anisotropic, either transversely isotropic with very low vertical permeability or azimuthally anisotropic with along-strike permeability (in the direction of faults and fractures created by the seafloor spreading process) being

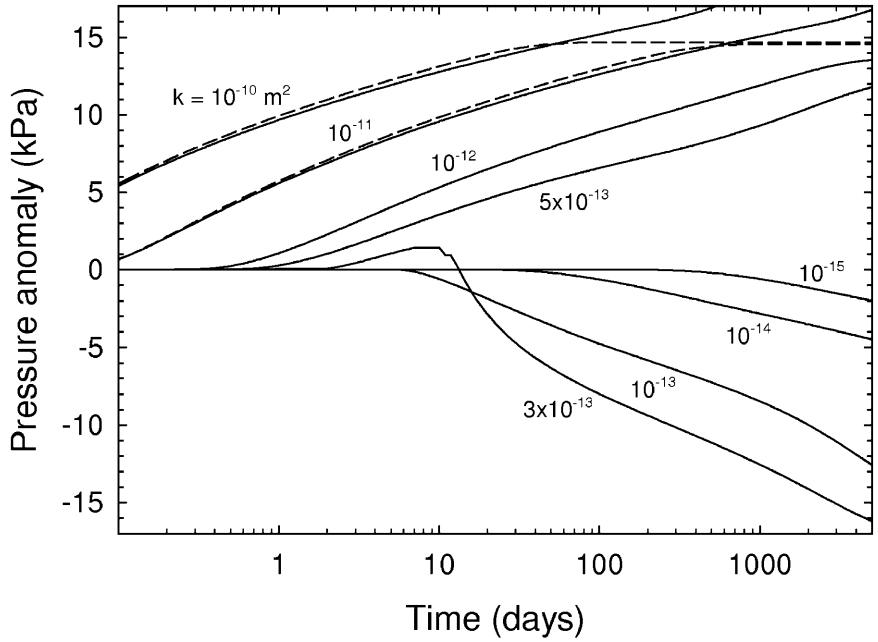

Figure 11. Upper basement pressure calculated at a distance of 2.5 km from a downhole flow perturbation source. Histories are shown for the case of flow into a 330 m thick isotropic basement layer over a range of permeability. Results assuming a free-flow radial boundary condition at 150 km and a no-flow boundary at 500 km are shown as dashed lines and solid lines, respectively. Results are insensitive to the depth of observation in the basement layer.

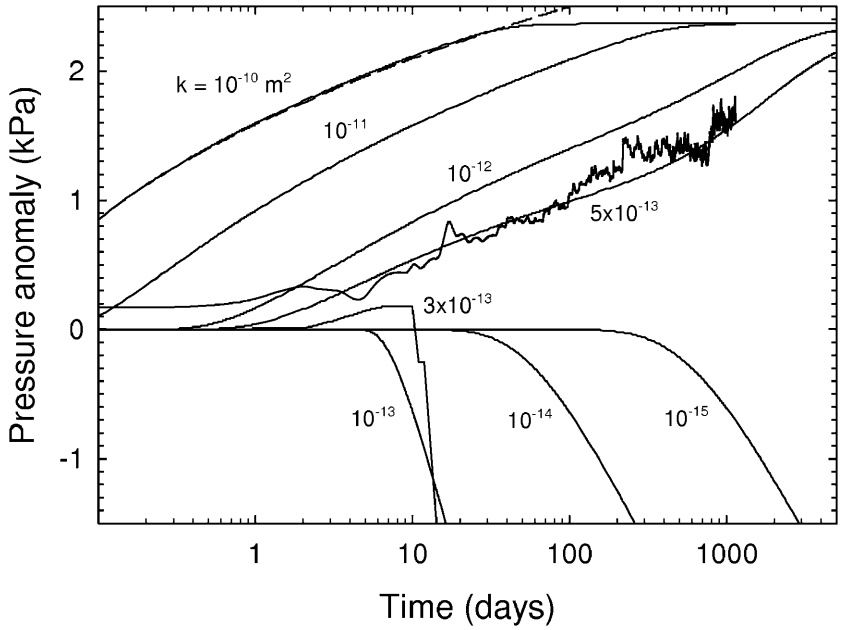

Figure 12. Plot equivalent to Figure 11, but for a 330 m thick transversely isotropic basement layer having zero effective vertical permeability, with pressures given at a depth of 12 m below the top of the basement layer. The pressure record observed at hole 1027C is shown for comparison. In this plot, results are shown for a domain with a free-flow boundary at 150 km; results with a no-flow boundary at 500 km are shown with the dashed line.

higher than cross-strike permeability. In a layered formation, flow can be absorbed just as efficiently as it can in a formation with isotropic properties– which provides conditions for sustained downhole flow over the same range of permeability– but the large anomalous pressures generated by negative buoyancy deep in the section (i.e., at hole 1301B) are inefficiently transmitted up to a shallow level of observation (i.e., at hole 1027C). The characteristics of the histories are the same, but the amplitudes of the anomalies are much smaller for the layered case. Results for an end-member model with no vertical permeability (Figure 12) shows that the observed record can be matched with a horizontal permeability of 5×10^{-13} m^2, a value not far above the threshold for runaway flow (which is the same as that for the istropic case, $\sim 3 \times 10^{-13}$ m^2).

[25] The case of azimuthal anisotropy was treated by *Fisher et al.* [2008] who calculated an "effective" permeability for a crust having varying degrees of anisotropy. It is treated in different but mathematically equivalent way here using the *Theis* [1935] analytic solution for an azimuthally anisotropic layer. The results show that, like the transversely isotropic case, the amplitude of the estimated perturbation at hole 1027C is diminished relative to the isotropic case, in agreement with the observed level (Figure 13), while still maintaining stable downhole flow via the high permeability in the along-strike direction. The predicted perturbation in the direction of hole 1026B would also be greatly diminished. This is consistent with the observations at hole 1026B, which show the formation pressure to be declining toward a level not very different from the estimated natural state (~20 kPa in late 2008 (Figure 3a) versus 18 kPa). Unfortunately, because of the unknown loss of pressure to leakage and the unknown thermal perturbation at that site, the observation at hole 1026B provides only a consistency check for this conclusion; quantitative conclusions cannot be made with confidence.

4.5. Signal Transit Time From Hole 1301A to 1027C

[26] To overcome the problems with applying the finite element model at early times, the Theis analytic solution has been used to gain independent constraints on permeability from the transit times implied from the delay between specific drilling "events" at hole 1301B and discrete anomalies observed at hole 1027C (see Figure 3e). Most clearly defined are (1) the pressure rise at hole 1027C that began soon after the initial phase of upper basement drilling at hole 1301B, with a transient peak occurring roughly 2 days after the hole reached its temporary completion depth of 85 msb, and (2) the transient that begins immediately after packer pumping tests in hole 1301B and reaches a peak roughly 2.5 days later. The implication for permeability is explored in Figure 14. This simulation examines the arrival time at a range of 2.4 km of a pressure transient from an impulsive source (distributed over the period of drilling operations or pump testing) as a function of permeability. The results suggest an effective permeability of the formation connecting the sites of $3–4 \times 10^{-13}$ m^2. Given the simplifying assumptions made for this and for the various models described above, the agreement among all the results is noteworthy.

5. Comparison With Other Estimates of Permeability and Implications

[27] A variety of determinations of upper crustal permeability have been made on the eastern Juan de Fuca Ridge flank, and previous comparisons of results from this and

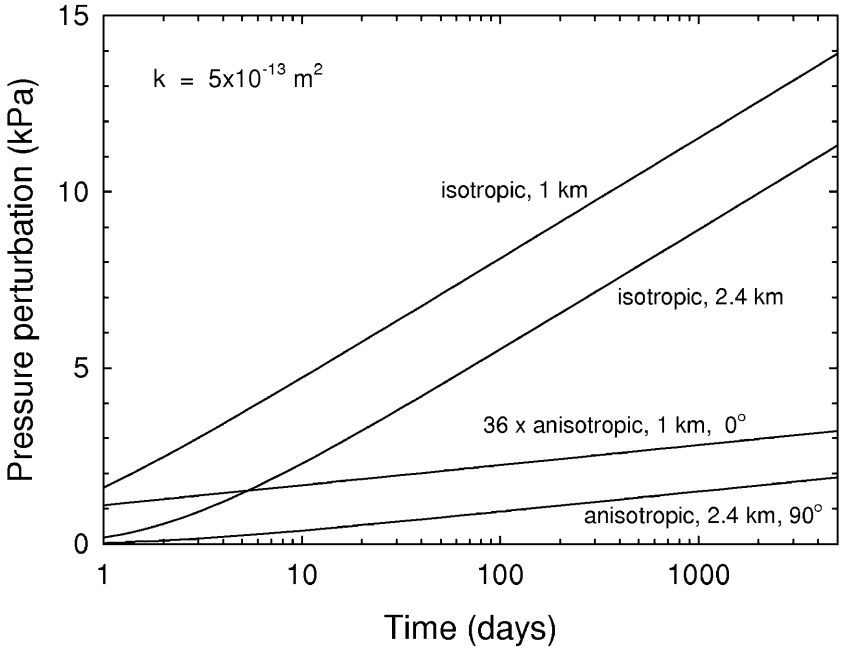

Figure 13. Pressure history predicted at distances of 1 and 2.4 km from an "injection" well following the Theis formulation [*Theis*, 1935; *Cooper et al.*, 1967] for media having isotropic and azimuthally anisotropic permeability. Solutions are given for directions parallel and perpendicular to the direction of high permeability. For the isotropic case, a permeability of 5×10^{-13} m^2 was assumed; for the anisotropic case, this value was assumed for the low-permeability direction (cross-strike) and a value 36 times higher than this for the along-strike direction.

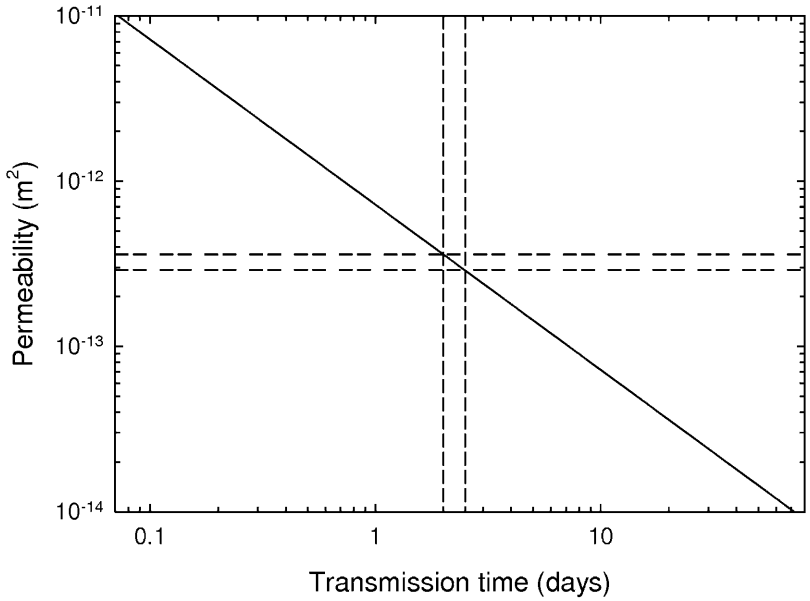

Figure 14. Transient hydrologic transmission time as a function of permeability calculated for the 2.4 km distance between holes 1301B and 1027C using a Theis formulation for radial flow. Vertical dashed lines show arrival times of the observed pulse peak at hole 1027C (Figure 3e) relative to the end of the first phase of drilling and of packer pumping tests in hole 1301B (Figure 3e) [*Becker and Fisher*, 2008]. Horizontal dashed lines show resulting range of inferred permeability.

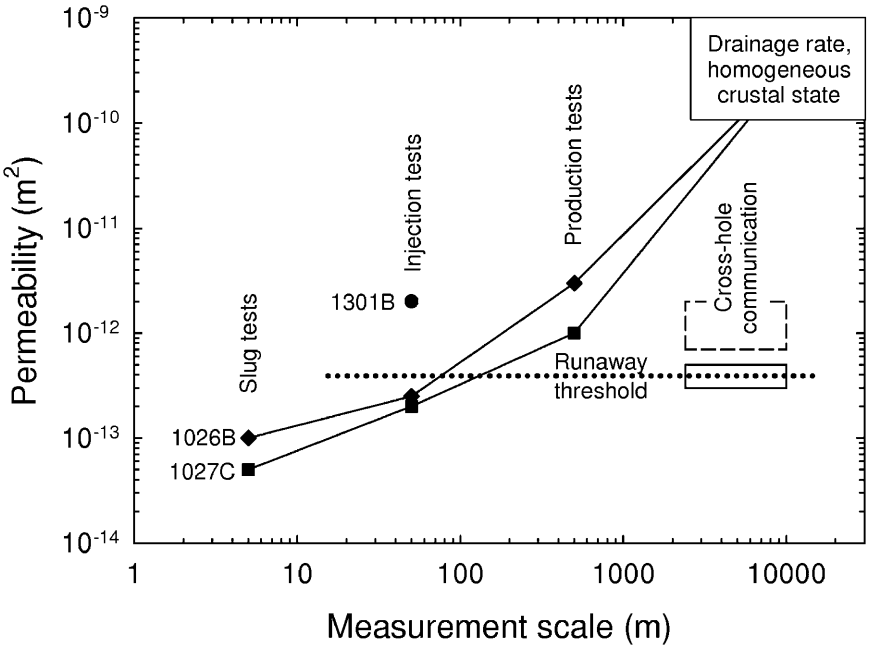

Figure 15. Permeability determinations in the area that is the focus of this paper as a function of approximate measurement scale, with the scale set by the characteristic durations of the measurements, ranging from minutes for packer slug tests, ~1 h for packer injection tests, days for production tests, and days to years for cross-hole communications. Determinations include ones from *Becker and Fisher* [2000], *Fisher et al.* [1997], *Becker and Davis* [2003], *Davis et al.* [2000], *Davis et al.* [2001], *Davis and Becker* [2002], *Spinelli and Fisher* [2004], and *Becker and Fisher* [2008]. The cross-hole communication determination shown as a dashed box is that of *Fisher et al.* [2008]; the solid box and the runaway flow threshold are from this paper.

other regions have led to several fundamental conclusions. These include (1) that permeability decreases with depth [*Becker*, 1989, 1990, 1991; *Fisher*, 1998; *Davis et al.*, 2004], (2) that permeability declines with increasing crustal age [*Fisher*, 1998; *Becker and Davis*, 2003], and (3) that effective permeability increases with the representative lateral scale of measurement [*Fisher*, 1998; *Becker and Davis*, 2003, 2004]. Observations presented in this paper have the potential to add insight to the last of these conclusions.

[28] A comparison of the results presented here to previous determinations in this same area is shown in Figure 15. This comparison is made via a format presented in the work of *Becker and Davis* [2003, 2004] that illustrates the general sensitivity of permeability to the scale of observation. Certain aspects of this comparison hold no surprises: (1) The injection test value determined in hole 1301B by *Becker and Fisher* [2008] falls above the threshold permeability required by the modeling results for sustained downhole flow. (2) The cross-hole permeability constrained by the drilling "impulse" transit time is in close agreement with that constrained by the long-term anomaly at 1027C. (3) Both of these estimates differ from that made by *Fisher et al.* [2008] on the basis of a subset of the same data, although given the differences between the nature of the calculations and the parameters used, some disagreement is to be expected. (4) The permeability values determined here from the long-term response at hole 1027C to flow in hole 1301B fall in a range between values determined in the individual holes 1027C and 1301B by borehole injection tests.

[29] In contrast to this general consistency, a large discrepancy is seen when the cross-hole communication determinations are compared to others made over a large scale (box labeled "drainage rate, homogeneous crustal state" in Figure 15). Despite the generally similar scale over which these various observations are sensitive and despite the fact that in both cases the effective permeabilities estimated apply primarily to the cross-strike direction, the cross-hole communication estimates fall roughly 3 orders of magnitude below the estimates based on observed postseismic strain drainage rates and on crustal temperature and pressure homogeneity. If the effective crustal permeability was as low as the cross-hole communications results suggest, lateral temperature and pressure variations in the crust would be much larger than observed and strain-induced changes in pressure would be preserved over much longer times than observed. One possible explanation for the inconsistency suggested by the comparison in Figure 15 is that the cross-hole results may be dominated by the hydrologic properties in the immediate vicinity of the "transmitting" and "receiving" boreholes and that there is relatively poor hydrologic communication from the boreholes to the fractures, faults, and volcanic horizons that allow highly efficient fluid and heat transport over large lateral distances.

[30] While perplexing, such a discrepancy may be instructive. Single-hole testing, cross-hole testing, and regional proxy analyses and modeling are sensitive to different aspects of crustal hydrogeology. Single-hole testing cannot be used to quantify azimuthal or vertical anisotropy but can resolve

layered heterogeneity near the borehole. Cross-hole testing can address anisotropy if there is a sufficient number of boreholes at appropriate depths and orientations, and can inform our understanding of crustal-scale properties if tests are run for a long enough time. And larger-scale analyses and modeling can help to elucidate effective properties across long distances. Any one of these methods alone is subject to numerous assumptions that require independent validation, (e.g., the dominant geometry of flow), but when interpreted together, they can lead to valuable new insights. Clearly the most productive approach to understanding crustal hydrogeology is to combine a wide variety of measurement, testing, and modeling approaches, to quantify agreement and differences in results, and, when necessary, to develop and apply new experimental and modeling techniques. The summary in Figure 15 demonstrates that a broad and integrated approach is needed in order to advance the study of a formation as hydrologically complex as the oceanic crust.

6. Summary and Conclusions

[31] Leakage through incomplete seals in the CORKed IODP borehole 1301B on the sedimented flank of the Juan de Fuca Ridge has provided unanticipated insight into the permeability structure of the upper igneous crust. Despite the natural superhydrostatic conditions at this location, downhole flow persisted for the observational period from July 2004 to August 2008. A numerical model for the situation shows that downhole flow can indeed be persistent when permeability exceeds a critical threshold. The value depends on the thickness of the layer that accepts flow, roughly 4×10^{-13} m^2 for the upper 318 m of the igneous section penetrated by hole 1301B or higher if flow is restricted to a layer thinner and shallower than the total depth of the hole. Applications of this general treatment can be done for other sites where overpressured sediment-buried basement formations were drilled (e.g., hole 858G where flow reversed only with the benefit of a CORK, and holes 896C, 1025C, and 1026B which all reversed within days with no restriction to flow). In each case, specific consideration must be given to factors such as the local geotherm, sediment thickness, basement penetration, and degree of natural local basement overpressure. The modeling carried out here can be applied directly to the situation at hole 1026B, and a quick check yields no surprise: With the depth of basement penetration at this site (48 m), the threshold for runaway downhole flow would be roughly 2×10^{-11} m^2 (Figure 8); permeabilities determined from pumping and production tests all fall well below this threshold (Figure 15).

[32] Independent information regarding basement permeability is provided by the response at the neighboring, properly sealed ODP hole 1027C 2.4 km away from the leaking hole 1301B. The transit time for impulsive signals generated at the time of drilling and pumping and the timing of the rise in pressure as a consequence of long-lived flow in hole 1301B suggest an effective permeability in the range of $3–5 \times 10^{-13}$ m^2. These estimates are similar to ones made previously by *Fisher et al.* [1997] and *Becker and Fisher* [2008] on the basis of single-hole production and injection tests and by *Fisher et al.* [2008] using a simplified analysis of the first year of the hole 1027C response to hole 1301B leakage, but all are much lower than values in the neighborhood of $10^{-10}–10^{-9}$ m^2 that have been inferred for the upper igneous crust in this area over a scale of many kilometers on the basis of the natural pressure and temperature state of the crust and the characteristic drainage time constant following crustal strain events [*Davis et al.*, 2001; *Davis and Becker*, 2002; *Spinelli and Fisher*, 2004]. The cause of this contrast is thought to be rooted in crustal heterogeneity. The high permeability that is inferred for the upper oceanic crust at a full-formation scale in the cross-strike direction may be contained in spatially infrequent subhorizontal layers and subvertical fractures that are not intersected by the boreholes.

[33] Although a good match is found between the timing of the simulated and observed pressure transients at hole 1027C, the estimated amplitude is much larger than that observed. Permeability anisotropy is shown to be a possible cause of the small observed amplitude. Either low permeability in the vertical direction or high in the along-strike direction, relative to the permeability in the cross-strike direction that connects the two holes, would cause diminished transient amplitudes at hole 1027C without affecting transit time. Whether the crust exhibits either or both could be studied using data from hole 1026B situated along strike from hole 1301B. Unfortunately, perturbations at that site arising from previous history, fluid sampling, and leakage preclude use of those data at the resolution required. Future remediation of the leak at hole 1026B would allow this hole to reequilibrate and make simultaneous cross-hole tests from hole 1301B to both hole 1027C and hole 1026B possible. In such a test, the speed of transmission of any transient from hole 1301B to hole 1026B would constrain permeability in the ridge-parallel direction, and if something like the hole 1301B runaway flow "experiment" were to be rerun, then the amplitude of the signal would provide an indication of the degree of vertical anisotropy as well. Although rates of flow will not be as great as that experienced in hole 1301B after IODP Expedition 301, controlled flow cross-hole experiments in both along- and across-strike directions are to be initiated in summer 2010 as part of IODP Expedition 327, using the four existing and two new holes. These experiments should provide additional insights regarding crustal-scale fluid flow, elastic properties, permeability anisotropy, and permeability heterogeneity.

[34] **Acknowledgments.** CORK observatory efforts have relied heavily on the technical expertise and support provided by Bob Meldrum, Bob Macdonald, and Tom Pettigrew by the shore-based and seagoing staff of the Ocean Drilling and Integrated Ocean Drilling Programs, by the captains and crews of the research vessels *Thompson* and *Atlantis*, and by the pilots and crews of the deep submergence research vehicle *Alvin* and the remotely operated vehicles *ROPOS* and *Jason*. Funding for the work has been provided by the Geological Survey of Canada, the U. S. National Science foundation through grants OCE-0400471, OCE-0727952, and OCE-0849354, and NEPTUNE-Canada.

References

Becker, K. (1989), Measurements of the permeability of the sheeted dikes in hole 504B, ODP Leg 111, *Proc. Ocean Drill. Prog., Sci. Results*, *111*, 317–325.

Becker, K. (1990), Measurements of the permeability of the upper oceanic crust at hole 395A, ODP Leg 109, *Proc. Ocean Drill. Prog., Sci. Results*, *106/109*, 213–222.

Becker, K. (1991), In-situ bulk permeability of oceanic gabbros in hole 735B, ODP Leg 118, *Proc. Ocean Drill. Prog.*, *118*, 333–347.

Becker, K., and E. E. Davis (2003), New evidence for age variation and scale effects of permeabilities of young oceanic crust from borehole thermal and pressure measurements, *Earth Planet. Sci. Lett.*, *210*(3–4), 499–508.

Becker, K., and E. E. Davis (2004), In situ determination of the permeability of the igneous oceanic crust, in *Hydrogeology of the Oceanic Lithosphere*, pp. 189–224, Cambridge Univ. Press.

Becker, K., and A. T. Fisher (2000), Permeability of upper oceanic basement on the eastern flank of the Juan de Fuca Ridge determined with drill-string packer experiments, *J. Geophys. Res.*, *105*(B1), 897–912, doi:10.1029/1999JB900250.

Becker, K., and A. T. Fisher (2008), Borehole packer tests at multiple depths resolve distinct hydrologic intervals in 3.5-Ma upper oceanic crust on the eastern flank of Juan de Fuca Ridge, *J. Geophys. Res.*, *113*, B07105, doi:10.1029/2007JB005446.

Becker, K., M. G. Langseth, and R. D. Hyndman (1984), Temperature measurements in hole 395A, Leg 78B, *Init. Repts. DSDP*, *78B*, 689–698.

Becker, K., M. G. Langseth, R. P. Von Herzen, R. N. Anderson, and M. Hobart (1985), Deep crustal geothermal measurements, hole 504B, DSDP Legs 69, 70, 83, and 92, *Init. Reps. DSDP*, *92*, 405–418.

Becker, K., R. H. Morin, and E. Davis (1994), Permeabilities in the Middle Valley hydrothermal system measured with packer and flowmeter experiments, *Proc. Ocean Drill. Prog., Sci. Results*, *139*, 613–626.

Becker, K., A. Bartetzko, and E. E. Davis (2001), Leg 174B synopsis: Revisiting hole 395A for logging and long-term monitoring of off-axis hydrothermal processes in young oceanic crust, *Proc. Ocean Drill. Prog., Sci. Results*, *174B*, 1–13.

Becker, K., E. E. Davis, F. N. Spiess, and C. P. deMoustier (2004), Temperature and video logs from the upper oceanic crust, holes 504B and 896A, Costa Rica Rift flank: Implications for the permeability of upper oceanic crust, *Earth Planet. Sci. Lett.*, *222*, 881–896.

Cooper, H. H., Jr., J. D. Bredehoeft, and I. S. Papadopulos (1967), Response of a finite diameter well to an instantaneous charge of water, *Water Resour. Res.*, *3*, 267–269.

Davis, E. E., and K. Becker (1994), Formation temperatures and pressures in a sedimented rift hydrothermal system: 10 months of CORK observations, holes 857D and 858G, *Proc. Ocean Drill. Prog., Sci. Results*, *139*, 649–666.

Davis, E. E., and K. Becker (2002), Observations of natural-state fluid pressures and temperatures in young oceanic crust and inferences regarding hydrothermal circulation, *Earth Planet. Sci. Lett.*, *204*(1–2), 231–248.

Davis, E. E., and K. Becker (2004), Observations of temperature and pressure: Constraints on ocean crustal hydrologic state, properties, and flow, in *Hydrogeology of the Oceanic Lithosphere*, pp. 225–271, Cambridge Univ. Press.

Davis, E. E., K. Becker, T. Pettigrew, B. Carson, and R. Macdonald (1992a), CORK: A hydrologic seal and downhole observatory for deep-sea boreholes, *Proc. Ocean Drill. Prog., Init. Reps.*, *139*, 45–53.

Davis, E. E., et al. (1992b), FlankFlux: An experiment to study the nature of hydrothermal circulation in young oceanic crust, *Can. J. Earth Sci.*, *29*, 925–952.

Davis, E. E., A. T. Fisher, and J. V. Firth, et al. (1997a), *Proc. Ocean Drill. Prog., Init. Reps.*, *168*, 470 pp.

Davis, E. E., K. Wang, J. He, D. S. Chapman, H. Villinger, and A. Rosenberger (1997b), An unequivocal case for high Nusselt-number hydrothermal convection in sediment-buried igneous oceanic crust, *Earth Planet. Sci. Lett.*, *146*, 137–150.

Davis, E. E., K. Wang, K. Becker, and R. Thomson (2000), Formation-scale hydraulic and mechanical properties of oceanic crust inferred from pore pressure to periodic seafloor loading, *J. Geophys. Res.*, *105*(B6), 13,423–13,435, doi:10.1029/2000JB900084.

Davis, E. E., W. Wang, R. E. Thomson, K. Becker, and J. F. Cassidy (2001), An episode of seafloor spreading and associated plate deformation inferred from crustal fluid pressure transients, *J. Geophys. Res.*, *106*, 21,953–21,963, doi:10.1029/2000JB000040.

Davis, E. E., K. Becker, and J. He (2004), Costa Rica Rift revisited: Constraints on shallow and deep hydrothermal circulation in oceanic crust, *Earth Planet Sci. Lett.*, *222*, 863–879, doi:10.1016/j.epsl.2004.03.032.

Duennebier, F., G. Blackinton, and J. Gieskes (1983), A man-made hot spring on the ocean floor, *Init. Repts. Deep Sea Drilling Proj.*, *65*, 357–359.

Fisher, A. T. (1998), Permeability within basaltic oceanic crust, *Rev. Geophys.*, *36*, 143–182.

Fisher, A. T., K. Becker, and E. E. Davis (1997), The permeability of young oceanic crust east of Juan de Fuca Ridge determined using borehole thermal measurements, *Geophys. Res. Lett.*, *24*(11), 1311–1314, doi:10.1029/97GL01286.

Fisher, A. T., T. Urabe, and A. Klaus (2005), *Proc. Integrated Ocean Drilling Prog., Exp. Repts.*, *301*, doi:10.2204/iodp.proc.301.103.2005.

Fisher, A. T., E. E. Davis, and K. Becker (2008), Borehole-to-borehole hydrologic response across 2.4 km in the upper oceanic crust: Implications for crustal-scale properties, *J. Geophys. Res.*, *113*, B07106, doi:10.1029/2007JB005447.

Gable, R., R. Morin, and K. Becker (1989), The geothermal state of hole 504B: ODP Leg 111 overview, *Proc. ODP, Sci Res.*, *111*, 87–96.

Morin, R. G., A. E. Hess, and K. Becker (1992), In situ measurements of fluid flow in DSDP holes 395A and 534A: Results from the DIANAUT program, *Geophys. Res. Lett.*, *19*(5), 509–512, doi:10.1029/91GL02947.

Mottl, M. J. (1989), Hydrothermal convection, reaction, and diffusion in sediments on the Costa Rica Rift flank: Pore water evidence from ODP Sites 677 and 778, *Proc. Ocean Drilling Prog., Sci. Res.*, *111*, 195–213.

Spinelli, G. A., and A. T. Fisher (2004), Hydrothermal circulation within topographically rough basaltic basement on the Juan de Fuca Ridge flank, *Geochem. Geophys. Geosyst.*, *5*, Q02001, doi:10.1029/2003GC000616.

Theis, C. V. (1935), The relationship between the lowering of the piezometric surface and the rate and duration of discharge of a well using ground-water storage, *Trans. AGU*, *16*, 519–524.

Wang, K. (2004), Applying fundamental principles and mathematical models to understand processes and estimate parameters, in *Hydrogeology of the Oceanic Lithosphere*, pp. 376–413, Cambridge University Press.

Wang, K., and E. E. Davis (1996), Theory for the propagation of tidally induced pore pressure variations in layered sub-seafloor formations, *J. Geophys. Res.*, *101*(B5), 11,483–11,495, doi:10.1029/96JB00641.

Wheat, C. G., and M. J. Mottl (1994), Hydrothermal circulation, Juan de Fuca eastern flank: Factors controlling basement water composition, *J. Geophys. Res.*, *99*(B2), 3067–3080, doi:10.1029/93JB01612.

K. Becker, Rosenstiel School of Marine and Atmospheric Science, University of Miami, Miami, FL 33149, USA.

E. E. Davis and J. He, Pacific Geoscience Center, Geological Survey of Canada, 9860 W. Saanich Road, Sidney, BC V8L 4B2, Canada. (edavis@nrcan.gc.ca)

A. Fisher, Earth and Planetary Sciences Department, University of California, Santa Cruz, CA 95064, USA.

A. LaBonte, Office of Energy Efficiency and Renewable Energy, U.S. Department of Energy, Washington, DC 20585, USA.